Two-dimensional distribution of volatiles in the lunar regolith from space weathering simulations

Dana M. Hurley[1], David J. Lawrence[1], D. Benjamin J. Bussey[1], Richard R. Vondrak[2], Richard C. Elphic[3], and G. Randall Gladstone[4]

[1]*Johns Hopkins University Applied Physics Laboratory, Laurel, MD, USA (dana.hurley@jhuapl.edu),* [2]*NASA Goddard Space Flight Center, Greenbelt, MD, USA,* [3]*NASA Ames Research Center, Moffett Field, CA, USA,* [4]*Southwest Research Institute, San Antonio, TX, USA*

Abstract: We present simulations of space weathering effects on ice deposits in regions of permanent shadow on the Moon. These Monte Carlo simulations follow the effects of space weathering processes on the distribution of the volatiles over time. The model output constrains the coherence of volatile deposits with depth, lateral separation, and time. The results suggest that ice sheets become broken and buried with time. As impacts begin to puncture an initially coherent surficial ice sheet, small areas with a deficit of ice compared to surrounding areas are formed first. As time progresses, holes become prevalent and the anomalous regions are local enhancements of ice concentration in a volume. The 3-D distribution is also heterogeneous because the ice is buried to varying depths in different locations. Analysis of the coherence of ice on 10 cm scales predicts that putative ice sheets in anomalous radar craters are < 100 Myr old. Surface frost becomes homogenized

within 20 Myr. The simulations show the data from the LCROSS impact and surrounding region are consistent with the ice deposit in Cabeus being >1000 Myr old. For future in situ analysis of cold trap volatiles, a horizontal range of 10 m is sufficient to acquire surface-based measurements of heterogeneously distributed ice. These results also support previous analyses that Mercury's cold traps are young.

1. Introduction

A question of both scientific and exploration interest is how water ice and other volatiles are distributed in permanently shaded regions (PSR) near the lunar poles. Practically, knowledge of volatile contents and their distribution in PSRs will aid in mission planning and design for future human and robotic lunar missions because those volatiles represent a significant potential resource. Scientifically, the PSRs potentially hold volatiles deposited over the last 2 billion years (Arnold, 1979; Siegler et al., 2011). This is an unparalleled, accessible record of volatile flux in the inner solar system.

Analysis of the possibility of water and other volatiles existing in PSRs has a long history (e.g., Urey, 1952; Watson et al., 1961; Arnold, 1979). Yet, the first spectroscopic confirmation of their presence inside PSRs came with the impact of the Lunar Crater Observation and Sensing Satellite (LCROSS) into Cabeus crater near the lunar south pole (Colaprete et al., 2010; Gladstone et al., 2010; Killen et al., 2010). Lunar data from the 1990s and 2000s provided evidence consistent with the presence of ice in the lunar polar regions; yet it was inconclusive. Neutron

47 spectroscopy from Lunar Prospector returned data consistent with the presence of
48 water ice in the near-subsurface of the Moon in permanently shadowed regions by
49 measuring heterogeneously distributed hydrogen concentrations at both lunar
50 poles (e.g., Feldman et al., 1998; Eke et al., 2009). Clementine and ground-based
51 radar returned tantalizing, but inconclusive evidence of ice in lunar PSRs (Nozette et
52 al., 1996; Campbell et al. 2006). Later, Mini-SAR and Mini-RF instruments on
53 Chandrayaan-1 and the Lunar Reconnaissance Orbiter (LRO) detected a radar
54 signature consistent with water ice in some polar craters on the Moon, but not all
55 PSRs (Spudis et al., 2010; Neish et al., 2011). Similarly, Lunar Exploration Neutron
56 Detector (LEND) on LRO also detected a heterogeneous distribution of hydrogen
57 among lunar PSRs (Mitrofanov et al., 2010). In addition, Lyman Alpha Mapping
58 Project (LAMP) on LRO detected far ultraviolet (FUV) spectra consistent with of
59 frost on the surface of some permanently shadowed regions (Gladstone et al., 2012).
60 Various measurements that are directly and/or indirectly sensitive to ice in
61 PSRs inherently have different sensitivities, fields of view, and resolution. Data from
62 different instruments often appear to be in conflict about the distribution of
63 volatiles they imply. E.g., the weakest spectral feature from LAMP was associated
64 with Shoemaker crater (Gladstone et al., 2012), which had the strongest hydrogen
65 feature from LEND (Sanin et al., 2012). The impact of LCROSS into Cabeus released
66 water and other volatiles (Colaprete et al., 2010; Gladstone et al., 2010; Killen et al.,
67 2010; Schultz et al., 2010), but abundances were higher than the background
68 amounts detected by neutron spectroscopy, implying heterogeneity within that PSR
69 either in area or in depth (Mitrofanov et al., 2010; Elphic et al., 2011).

To add another level of complication, volatiles emplaced in lunar polar regions are modified over time by space weathering processes including impact gardening (e.g., Arnold, 1979). Temperatures below 90 K are too low for thermal diffusion and sublimation (e.g. Vasavada et al., 1999; Andreas, 2007; Schorghofer and Taylor, 2007; Paige et al., 2010; Siegler et al., 2011); however, volatiles deposited in lunar cold traps are subjected to other destructive mechanisms (Arnold, 1979). It is important to understand the modification processes on several different scales in order to interpret disparate data in a consistent manner. We present a simulation and sample the results to provide a self-consistent, multi-dimensional view of lunar polar volatiles. This work suggests that the lateral coherence, a property necessary for radar detection of ice, disappears quickly. The oldest ice deposits, invisible to radar, still can produce a signature observable by neutron spectroscopy. Spectroscopy in the ultraviolet can provide crucial input for determining any recent or steady state delivery of volatiles.

2. Model

An ice layer in a cold trap, even if is initially homogeneous, is disrupted by impact gardening. Impacts can act to remove volatiles as well as preserve volatiles. As impacts emplace an ejecta blanket, the layer protects volatiles that had been exposed to the surface from losses to sputtering and sublimation. However, impacts vaporize material, thereby releasing volatiles at the point of impact. As each location on the Moon has undergone a unique impact history, this process introduces heterogeneity into the system.

93 We incorporate techniques developed to analyze Apollo drill cores (Arnold,
94 1975; Borg et al., 1976) to create a Monte Carlo model that examines the evolution
95 of ice in a permanently shaded region on the Moon (Crider and Vondrak, 2003a;
96 2003b) and Mercury (Crider and Killen, 2005). Previously, the model simulated the
97 evolution over time of ice with depth in a single vertical column of regolith. We
98 have expanded the model to investigate lateral scale lengths of properties of ice.
99 Instead of simulating a single column, we now simulate two columns with
100 adjustable lateral separation. We consider impacts and gardening in the area
101 including the pair of columns and allow any impact to affect whichever simulation
102 columns are in the crater radius or ejecta blanket. Correlations between columns
103 provide a look at how features persist in both time and distance.

104 The model starts with an initial configuration of water ice. Here, we use a
105 coherent layer of ice on the surface of a given thickness and concentration. The
106 Monte Carlo simulation implements impacts by randomly generating a set of
107 discrete impacts using the frequency and size distribution of impacts of $m > 1$ μg
108 (Neukum et al., 2001). When a discrete impactor hits, its location relative to each
109 column of regolith is computed. The model adds or removes material appropriate
110 for the associated crater. The excavation/ejecta layer is handled consistently
111 between the columns. If material is removed from one column and emplaced on the
112 other, the concentration of volatiles in the excavated material factors into the
113 concentration of volatiles in the ejecta layer assuming a variable volatile loss from
114 the impact. The simulations provide a simple approximation of impact cratering
115 that neglects some important aspects of cratering, including compaction and

116 slumping. Smaller impactors are treated as an average accumulation between
117 larger, discrete impacts (Gault et al., 1972) because computation time for handling
118 these discretely increases while the effects of the impacts become smaller. Volatiles
119 at the surface can be lost during exposure to photolysis or sputtering. Thermal
120 diffusion is neglected because the rate is small for T < 90 K (Schorghofer and Taylor,
121 2007). That limits this application to the coldest areas on the Moon.

122 Each model run presented in this paper starts with an initial ice layer on the
123 surface that is 10 cm thick and comprised of 100 wt.% water ice. This is more
124 concentrated than expected, but the results scale with the assumed initial weight
125 fraction of ice. A set of 1000 pairs of columns was run for each lateral separation (1
126 cm, 10 cm, 1 m, 10 m, 100 m, 1 km). The water concentration as a function of depth
127 for each pair is recorded at times 1, 2, 5, 10, 20, 50, 100, 200, 600, and 1,000 Myr
128 after the ice layer is emplaced.

129

130 **3. Results**

131 Each Monte Carlo run represents a possible scenario given the inputs to the
132 program. Running 1000 cases with the same program inputs but a different seed to
133 the random generator produces a set of profiles that are representative of what can
134 be expected to occur on the Moon. In general, impacts act to cover the ice layer
135 because the area of the ejecta blanket is larger than the area of the crater. Thus each
136 location on the Moon statistically receives more burial events than excavation
137 events. In any individual run, the ice layer tends to stay intact; buried under a

thickness of ejecta. The thickness of the ejecta layer varies from case to case; but the burial rate is 1 mm/Myr on average.

On average, excavation events are deeper than the burial events. Furthermore, excavation events potentially disrupt the ice layer. Excavation removes a fraction of the ice deposit. The resulting ice layer is thinner than the original. The ice concentration in underlying regolith is nearly the same as the original concentration because of the way the code implements an impact. An impact that is large enough to penetrate the ice layer will also affect the adjacent column of material on the lateral scale determined by the depth to diameter ratio of impact craters. As impacts begin to puncture the ice layer, there will be well-correlated areas of decreased ice concentration compared to the surroundings. Both the number of these holes and the size of these holes increase with time as more and larger impacts become likely. As time progresses, buried ice and holes become prevalent and the few undisturbed sections of ice are rare. Thus at later times, the anomalous regions should be expected to have higher ice content than their surroundings.

Figure 1 shows the heterogeneity as a function of depth and column separation. The difference between the ice content in each depth bin for column 1 from that in the same depth bin for column 2 is calculated. The standard deviation, defined here as the sum of the squared differences for each of the 1000 runs divided by the number of runs, is shown for each depth bin at ages (from left to right) 1 Myr, 10 Myr, 100 Myr, and 1000 Myr as a function of lateral separation. Low standard deviation means that the ice layer is still uniform (e.g., the dark area at the top in the

161 left plot) or that there is a homogeneous layer that lacks ice (e.g., the dark area at
162 the bottom of the left plot). The high deviations at the top and bottom of the
163 enriched ice layer show the depths at which some columns have ice and others do
164 not. The surface becomes homogeneous with low water concentration (f_{ice} < 1
165 wt.%) at t ~ 20 Myr. Deviations in the ice layer increase with lateral separation in
166 the 100 Myr case and at later times. Samples separated by >1 m would have very
167 different vertical profiles for deposits aged > 100 Myr.

168 The next analysis studies the occurrence of dry regions. In Figure 2, for each
169 of the 1000 runs of 100 Myr and 1 m lateral separation, a data point appears
170 showing the average ice content in the top meter of Column 1 vs. Column 2. Four
171 populations appear. The upper right group includes runs in which both columns
172 retained a significant amount of ice. The population in the upper left is where
173 column 2 retained ice, but column 1 lost the ice after an impact. The converse holds
174 for the constituents in the lower right. The lower left contains the trials where the
175 ice is removed from both columns. The individual profiles of ice content as a
176 function of depth are widely varied in the set of runs, reflecting varying burial
177 depths and thicknesses of retained ice. However, the concentration of the ice, where
178 it is retained, does not change much from column to column or from the original
179 value.

180 The number of points in the upper left, upper right, and lower right
181 comprises the number of runs in which at least one of the two columns is "wet,"
182 which we define here as having an average of 1 wt. % ice over a given depth.
183 Dividing the number of points in the shaded area by the total number of runs gives

184 the probability of finding at least one wet spot through sampling two columns at
185 that lateral separation.

186 These probabilities are given in Figure 3 as a function of lateral separation
187 and age of the deposit. Note that this simulation assumes that the ice layer began as
188 a 10-cm thick sheet of pure ice and that thermal diffusion is negligible. At most
189 ages, the probability is higher with increased lateral separation up to separations of
190 10 m. Greater separation does not improve the probability.

191 Next we determine the probability of retaining a solid block of ice (Figure 4.)
192 The condition chosen for coherence is that there is a large abundance of ice (f_{ice} >
193 0.5) and that the difference between the abundance in the two columns is small
194 compared to the average value ($|f_{ice}(A) - f_{ice}(B)| < 0.2 < f_{ice} >$). Coherence on the
195 size scale on order of the radar wavelength produces a strong radar circular
196 polarization ratio (CPR) enhancement (e.g., Spudis et al., 2010). For Mini-RF and
197 Mini-SAR, the relevant scale is ~10 cm. Integrated over the original depths
198 containing ice, the lateral correlation decreases with age. The probability of 10-cm
199 size ice blocks remaining as a function of age can be fit by the function $P_{block} = 0.904 - \log(t)/3.108$. Detectable ice blocks should remain for ~100 Myr. The ice blocks
200
201 become too small by 100 Myr.
202

203 **4. Discussion**

204 Owing to the spatial resolution of orbital neutron spectroscopy, large area
205 averages from the model runs are the best representation of neutron data. Neutron
206 spectroscopy, which is sensitive to about 1 m depth, would therefore be detecting

207 ice that has been deposited within the last 1000 Myr. These older deposits have a
208 high degree of heterogeneity in both depth and lateral distribution. If several ice
209 layers exist and one is on the surface, the standard dry-over-wet model used to
210 convert neutron spectra into water abundances might underestimate the water
211 abundance (Lawrence et al., 2011). Thus, quantifying the ice in a surface layer could
212 improve models of neutron leakage used in converting neutron spectra to water
213 abundances.

214 Surface frost could appear two ways. First, it could be steadily deposited by
215 volatiles migrating from other areas on the Moon. This case was studied by Crider
216 and Vondrak (2003a) and is not addressed here. Secondly, volatiles on the surface
217 can result from a partially buried ice layer, which may have resulted from episodic
218 sources such as cometary impacts. As space weathering affects the surface more
219 than it does the subsurface, surface abundances decrease rapidly without additional
220 input. The model suggests that in the top 1 mm, values are heterogeneous soon
221 after emplacement as ejecta slowly cover the layer and losses to space occur
222 through photolysis and sputtering. The heterogeneous period is brief; and the
223 surface frost becomes homogeneously low within a few 10 Myr after deposition. The
224 presence of surface frost would likely imply the addition of volatiles at a steady rate.
225 The concentration of surface frost could be used to constrain the rate of source/loss
226 to the PSRs.

227 Lateral coherence disappears quickly on the 20-cm scale according to these
228 simulations. This implies that ice deposits in anomalous craters in the north polar
229 region (Spudis et al., 2010) would be young features—less than 100 Myr—if the

features initially began as a 10 cm thick layer and if thermal diffusion is negligible. A thicker initial layer would take longer to break apart to the point of losing the high-CPR radar signature. However, thicker initial deposits require a large source. The model suggests that ice deposits in the larger cold traps including Cabeus, which lack a high-CPR radar signature, are older than 100 Myr old or started as layers thinner than those detectable by radar.

Schultz et al. (2010) concluded that the LCROSS impact excavated a 20-30 m diameter crater. Timing of the observations of water ice is consistent with the water being derived from a depth of 2-3 m. Furthermore, Mitrofanov et al. (2010) state that the impact region is enriched in water by a factor of ~2 compared to the surrounding area. This study defines "enriched" as both columns containing ice amounts greater than the average ice amount found from the set of runs. The likelihood of two columns separated by 10 m being enriched to that degree is negligible until the deposit is 1000 Myr old (see supplemental material). Alternatively, the enrichment could occur with depth. Neutron spectroscopy is not sensitive to ice buried below 1-m of regolith. If the ice deposit in Cabeus is buried significantly below the depth to which neutrons are sensitive, this modeling would suggest that the ice deposit is older than 1000 Myr. These findings are more stringent than the constraint implied by the lack of radar CPR enhancement.

5. Conclusions

Data on many spatial scales indicate that ice in lunar polar regions has a heterogeneous distribution. Space weathering, especially impact gardening,

253 introduces heterogeneity even if an ice deposit is homogeneous initially. This
254 process takes time, thus the degree of heterogeneity is related to the age of the
255 deposit. Comparing models to data suggests that the ice deposits in lunar polar
256 regions are generally old and generally buried. Possible exceptions do exist in the
257 high CPR crater floors in the northern polar region, which are consistent with
258 younger ages than deposits in the larger cold traps. Surface frost could indicate that
259 there are some continually delivered volatiles.

260 The next steps in lunar polar exploration are to characterize the deposits
261 with in situ compositional and depth analysis. The heterogeneity due to space
262 weathering guarantees that lateral variations will exist; and a static lander might
263 have the misfortune of landing in a dry spot. These simulations suggest that a
264 lateral range of ~10 m is optimal in the trade between minimizing the probability of
265 probing a dry spot and minimizing mission duration. These simulations assumed
266 that the ice layer began as a 10 cm-thick layer. Other initial conditions would
267 produce different probabilities. Mass spectroscopy would identify constituents,
268 which likely include multiple sources. With a small number of samples with depth,
269 one could reliably determine what the peak concentration of the ice deposit was
270 when it was emplaced, assuming thermal diffusion does not play a role. Although
271 the age cannot be determined with one or two depth samples, increasing the
272 number of depth distributions taken can increase the significance of the age inferred
273 using the burial rate.

274 The modeling described here has application to other airless bodies,
275 including Mercury. Mercury's cold traps are inherently different than the Moon's in

276 that radar observations are consistent with every permanently shadowed region
277 containing relatively pure ice (Slade et al., 1992). They are interpreted to be young
278 (Crider and Killen, 2005). This study supports the conclusion that Mercury's
279 deposits are young, assuming that the volatiles have never been thermally
280 mobilized. As MESSENGER acquires data, a stronger comparison between the Moon
281 and Mercury can be made.
282
283 **Acknowledgements:** This work was supported by the NASA Lunar Science
284 Institute and LASER program through grants NNA09DB31A and NNX08BA60G.
285
286 **References**
287 Andreas, E. L. (2007) New estimates for the sublimation rate for ice on the Moon,
288 *Icarus 186*, 24-30.
289 Arnold, J. R. (1975) Monte Carlo simulations of turnover processes in the lunar
290 regolith, *Proc. Lunar Sci. Conf. 6th*, pp. 2375-2395.
291 Arnold, J. R. (1979) Ice in the lunar polar regions, *J. Geophys. Res., 84*, pp. 5659-5668.
292 Borg, J., G. M. Comstock, Y. Langevin, et al. (1976) A Monte Carlo model for the
293 exposure history of lunar dust grains in the ancient solar wind, *Earth Plan. Sci.*
294 *Lett., 29*, pp. 161-174.
295 Campbell, D. B., B. A. Campbell, L. M. Carter, J-L Margot, N. J. S. Stacy (2006) No
296 evidence for thick deposits of ice at the lunar south pole, *Nature 443*,
297 doi:10.1038/nature05167.

298 Colaprete, A., P. Schultz, J. Heldmann, et al. (2010) The detection of water within the
299 LCROSS ejecta plume, *Science 330*, 463-468.
300 Crider, D., and R. Killen. (2005) Burial rate of Mercury's polar volatile deposits,
301 *Geophys. Res. Lett. 32* (12): L12201, doi:10.1029/2005GL022689.
302 Crider, D. H., and R. R. Vondrak (2003a) Space weathering effects on lunar cold trap
303 deposits, *J. Geophys. Res. 108* (E7): 5079, 10.1029/2002JE002030.
304 Crider, D. H., and R. R. Vondrak. (2003b) Space Weathering of ice layers in lunar
305 cold traps, *Adv. Space Res. 31* (11): 2293-2298.
306 Eke, V. R., L. F. A. Teodoro, and R. C. Elphic (2009) The spatial distribution of polar
307 hydrogen deposits on the Moon, *Icarus*, 200, 1, 12 – 18.
308 Elphic, R. C., et al. (2011) The average water concentration within Cabeus crater:
309 Inferences from LRO/Diviner, LCROSS and Lunar Prospector, *Lunar Planet.*
310 *Sci. Conf., 42,* abstract #2751.
311 Feldman, W. C., S. Maurice, A. B. Binder, et al. (1998) Fluxes of fast and epithermal
312 neutrons from Lunar Prospector: evidence for water ice at the lunar poles,
313 *Science, 281,* pp. 1496-1500.
314 Gault D. E., F. Horz, and J. B. Hartung. (1972) Effects of microcratering on the lunar
315 surface, *Geochim. Cosmochim. Act. 3*, pp. 2713-2734.
316 Gladstone, G. R., D. M. Hurley, K. D. Retherford, et al. (2010) LRO-LAMP
317 Observations of the LCROSS Impact Plume, *Science 330*, 472-476.
318 Gladstone, G. R., K. D. Retherford, A. F. Egan, et al., (2012) Far-Ultraviolet Reflectance
319 Properties of the Moon's Permanently Shadowed Regions, *J. Geophys. Res. 117*,
320 E00H04, doi:10.1029/2011JE003913.

321 Killen, R. M., A. E. Potter, D. M. Hurley, C. Plymate, and S. Naidu, (2010) Observations
322 of the Lunar Impact Plume from the LCROSS Event, *Geophys. Res. Lett. 37*,
323 L23201, doi:10.1029/2010GL045508.
324 Lawrence, D. J., D. M. Hurley, W. C. Feldman, et al. (2011) Sensitivity Of Orbital
325 Neutron Measurements To The Thickness And Abundance Of Surficial Lunar
326 Water, *J. Geophys. Res., 116*, E01002, 10.1029/2010JE003678.
327 Mitrofanov, I. G., A. B. Sanin, W. V. Boynton, et al., (2010) Hydrogen Mapping of the
328 Lunar South Pole Using the LRO Neutron Detector Experiment LEND, *Science*
329 *330*, 483-486.
330 Neish, C. D., D. B. J. Bussey, P. Spudis, et al. (2011) The nature of lunar volatiles as
331 revealed by Mini-RF observations of the LCROSS impact site, *J. Geophys. Res.*
332 *116*, E01005, doi:10.1020/2010JE003647.
333 Neukum, G., B. A. Ivanov, and W. K. Hartmann (2001) Cratering records in the inner
334 solar system in relation to the lunar reference system, *Space Sci. Rev. 96*,
335 pp.55-86.
336 Nozette, S., C. L. Lichtenberg, P. Spudis, et al. (1996), The Clementine bistatic radar
337 experiment, *Science, 274*, 1495–1498
338 Paige, D. A., M. A. Siegler, J. A. Zhang, P. O. Hayne, et al. (2010) Diviner Lunar
339 Radiometer Observations of Cold Traps in the Moon's South Polar Region,
340 *Science 330*, 479-482.
341 Sanin, A. B., et al. (2012) Testing of lunar permanently shadowed regions for water ice,
342 *43rd Lun. Planet. Sci. Conf.*, 1659.

343 Schorghofer, N., and G. J. Taylor (2007) subsurface migration of H_2O at lunar cold traps,
344 *J. Geophys. Res. 112* (E2) E02010.
345 Schultz, P. H., B. Hermalyn, A. Colaprete, K. Ennico, M. Shirley, and W. S. Marshall
346 (2010) The LCROSS Cratering Experiment, *Science 330*, 468-472.
347 Slade, M. A., B. J. Butler, and D. O. Muhleman (1992), Mercury radar imaging—
348 Evidence for polar ice, *Science, 258*, 635–640.
349 Spudis, P. D., et al. (2010), Initial results for the north pole of the Moon from
350 Mini-SAR, Chandrayaan-1 mission, *Geophys. Res. Lett. 37*, L06204,
351 doi:10.1029/2009GL042259.
352 Urey, H. C. (1952) *The Planets, Their Origin and Development*, Yale Univ. Press, New
353 Haven, pp. 17-18.
354 Vasavada, A. R., D. A. Paige, S. E. Wood. (1999) Near-surface temperatures on
355 Mercury and the Moon and the stability of polar ice deposits, *Icarus, 141*, pp.
356 179-193.
357 Watson, K., B. C. Murray, and H. Brown (1961) The behavior of volatiles on the lunar
358 surface, *J. Geophys. Res., 66*, pp. 3033-3045.
359
360 **Figure Captions**

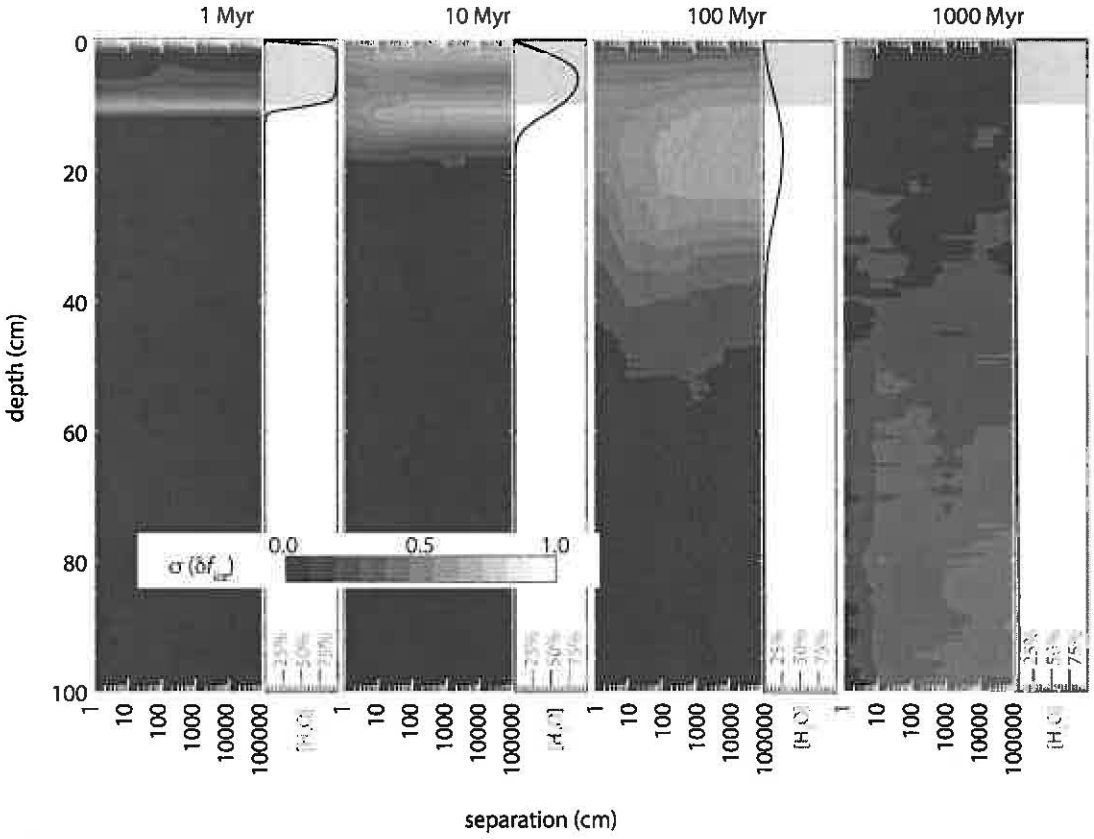

361

362 Figure 1. The standard deviation of the value of the concentration of ice as a function
363 of depth in one column compared to another column separated by the amount on
364 the x-axis for an ice layer that was 10 cm thick to start after (from left to right) 1
365 Myr, 10 Myr, 100 Myr, and 1000 Myr. For reference, the average concentration for
366 the age is provided to the right of each plot.

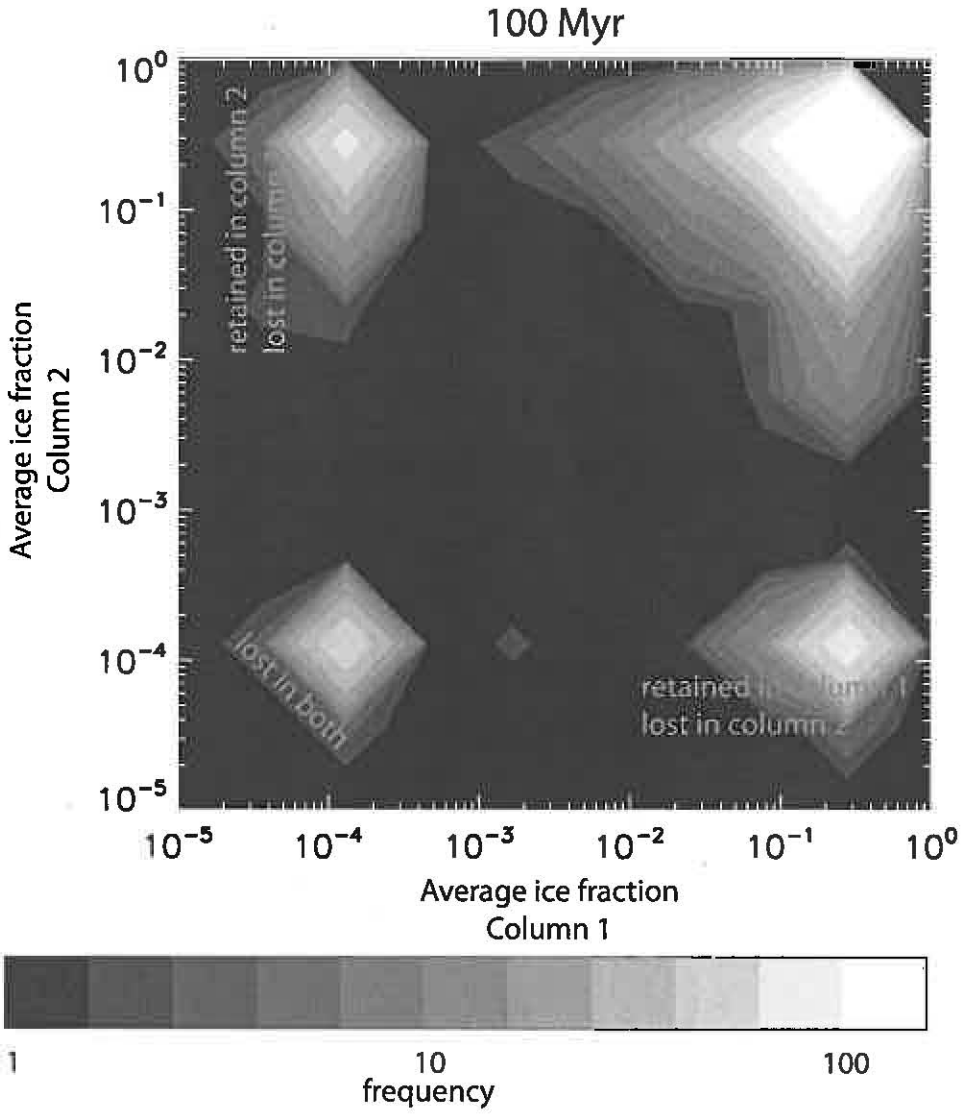

367

368 Figure 2. The integrated ice content in one column versus the other column from a

369 set of 1000 runs of 100 Myr and 1 m separation.

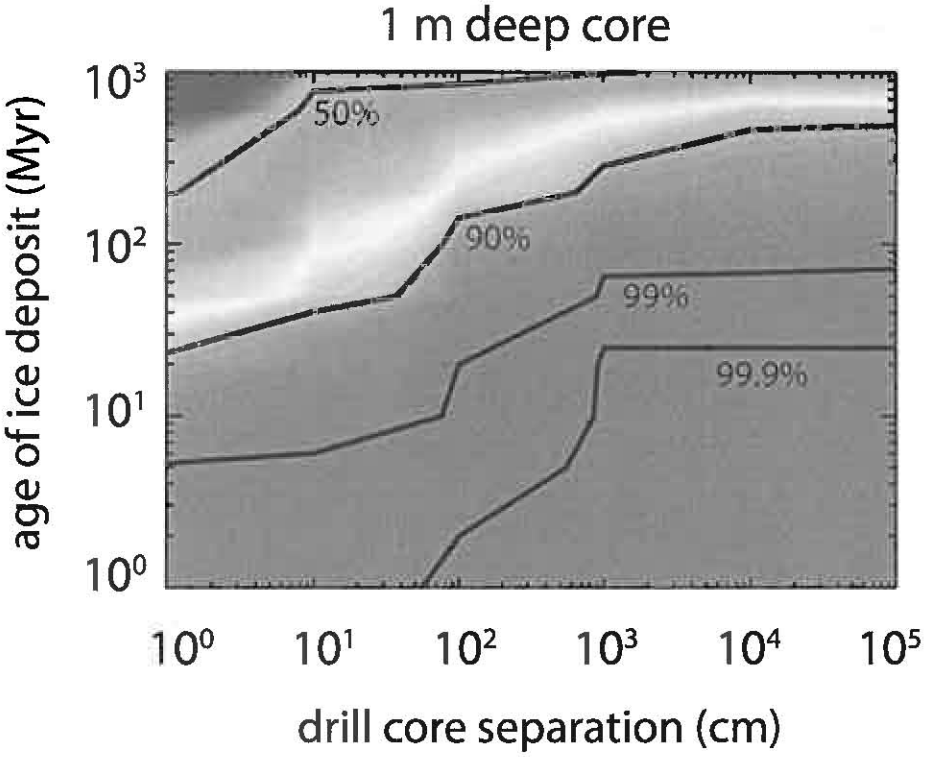

370

371 Figure 3. The probability that at least one drill of two drill cores has a measurable
372 amount of water as a function of the age of the deposit and the lateral separation of
373 the two cores. For deposits that are younger than 100 Myr, the probability
374 improves with displacement up to a distance of 10 m. Greater distances do not
375 significantly increase the probability of finding the ice.

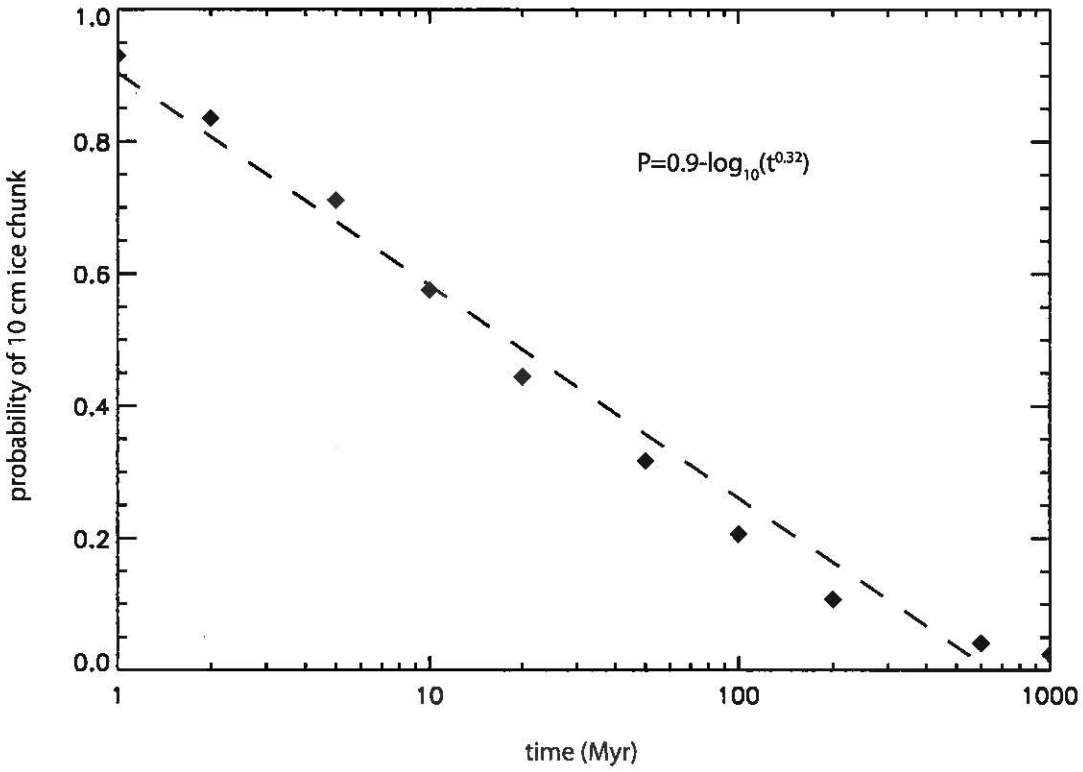

376

377 Figure 4. Integrating the ice abundance over original depth from the model runs
378 then counting the occurrence rate that the ice abundance is large and is similar to
379 the ice abundance in the adjacent column provides the probability that an ice block
380 is retained. For the ice in the top 20 cm, the occurrence rate of 10 cm wide ice
381 blocks decreases with time.

382